CHIN. PHYS. LETT. Vol. 38, No. 2 (2021) 024401

Tuning Thermal Conductivity in Si Nanowires with Patterned Structures

Gui-ping Zhu(朱桂萍), Chang-wei Zhao(赵长伟), Xi-wen Wang(王希稳), and Jian Wang(王健)*

College of Physical Science and Technology, Yangzhou University, Yangzhou 225002, China

(Received 10 October 2020; accepted 4 December 2020; published online 27 January 2021)

Tuning the thermal conductivity of silicon nanowires (Si-NWs) is essential for realization of future thermoelectric devices. The corresponding management of thermal transport is strongly related to the scattering of phonons, which are the primary heat carriers in Si-NWs. Using the molecular dynamics method, we find that the scattering of phonons from internal body defects is stronger than that from surface structures in the low-porosity range. Based on our simulations, we propose the concept of an exponential decay in thermal conductivity with porosity, specifically in the low-porosity range. In contrast, the thermal conductivity of Si-NWs with a higher porosity approaches the amorphous limit, and is insensitive to specific phonon scattering processes. Our findings contribute to a better understanding of the tuning of thermal conductivity in Si-NWs by means of patterned nanostructures, and may provide valuable insights into the optimal design of one-dimensional thermoelectric materials.

DOI: 10.1088/0256-307X/38/2/024401

Thermoelectric features of nanowires[1–4] have attracted a great deal of attention in recent decades due to their unique electrical and thermal properties. It is worth noting that energy conversion efficiency is an important parameter with respect to the characterization of the combined electrical and thermal properties of thermoelectric materials, which can then be measured by thermoelectric figures of merit.[5–8] Significantly, compared with other thermoelectric materials, the thermal conductivity of silicon nanowires (Si-NWs) can be effectively controlled (i.e., by increasing its energy conversion efficiency[9,10]) via the appropriately low-cost engineering of self-nanostructures.

A large number of experimental,[11–14] theoretical, and numerical methods[15–22] have been employed to explore the effects of nanostructures[3,23] on thermal conductivity in Si-NWs. These patterned nanostructures may include isotope impurities,[24] superlattices,[25] core-shell or coating structures,[26] rough surfaces,[9,10,27] or internal defects.[28–31] Although a considerable amount of research[3,4,23–30] in recent years has been dedicated to tuning the thermal conductivity of Si-NWs, the mechanism of phonon scattering by nanostructures, and, in particular, the difference between rough surfaces and internal patterned structures, is not yet thoroughly understood, and needs to be clarified.

In this work, we explore the differences between surface scattering and internal defect scattering of phonons in nanostructure-patterned Si-NWs. It is found that the scattering of phonons from internal body-defects is stronger than that from surface structures in the low-porosity range. Based on our simulations, an exponential decay in thermal conductivity with porosity is proposed. Our calculations are consistent with recent experimental observations,[12] and may provide valuable insights into the optimal design of one-dimensional thermoelectric materials.

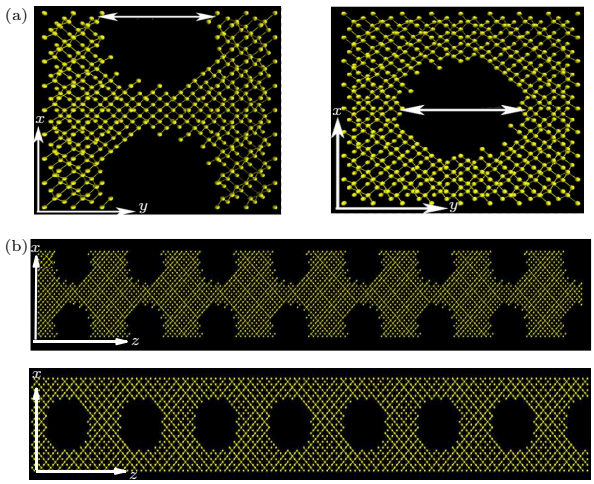

Fig. 1. Snapshot of Si-NWs with patterned nanostructures. (a) Cross-sectional areas of Si-NWs with surface pores (left) and internal pores (right). (b) Longitudinal profiles of Si-NWs with surface pores (upper) and internal pores (lower) along the z axis.

Models and Computational Methodology. Figure 1 shows the schematic of our Si-NW model system with patterned nanostructures. The longitudinal direction for heat flow is set along the z axis, while the transverse cross-section is selected for the x and y directions. To obtain the patterned structures of the nanowire, the atoms in the regime of the patterned sphere are removed. Thus, a spherical pore corresponds to a set of missing atoms. The center of the

Supported by the National Natural Science Foundation of China (Grant No. 11875047).
*Corresponding author. Email: wangjian@yzu.edu.cn
© 2021 Chinese Physical Society and IOP Publishing Ltd

internal spherical pore is located in the center of the nanowire, while the center of the pore with respect to surface defects is at the nanowire surface. The nanostructured spheres are further periodically assembled along the longitudinal z-direction, as illustrated in Fig. 1(b). To quantify the volume of the patterned sphere-pore, the porosity is defined as the ratio of the number of removed atoms in the pores to the total number of atoms in a corresponding perfect nanowire.

For our simulations, we select a square cross-sectional area of $3.26 \times 3.26\,\mathrm{nm}^2$, and the length of the nanorod is set to 108.62 nm. We adopt this nanorod model to simulate thermal transport in nanowires in our experiments. We have simulated some longer nanowires with larger cross-sections, but have found that longer lengths, up to 400 nm, and a wider cross-section did not significantly affect the results. This is consistent with previous reports.[32–34] Our selection of this specific size and length of nanowires takes into account the significant computational requirements of this simulation, in the face of limited computing resources. We investigate the thermal conductivity of Si-NWs with porosity ranging from 0% (perfect Si-NWs) to 30.64%.

Classical molecular dynamics simulations have been widely used to estimate thermal conductivity. In this Letter, we use the reverse non-equilibrium molecular dynamics (RNEMD) method, as presented by Müller–Plathe.[35,36] This is implemented using the large-scale atomic/molecular massively parallel simulator (LAMMPS) software package.[37] The heat source and the heat sink are placed in the middle slab of ribbon and at one end slab of the ribbon, respectively. Periodical boundary conditions are applied along the longitudinal direction of the ribbon, while the shrink-wrapped boundary condition[37] is taken in the transverse directions. A symmetrical temperature gradient ∇T is established along the direction of heat flow by exchanging the kinetic energies between the hottest atom in the heat source and the coldest atom in the heat sink. This energy exchange leads to a heat flux J between the cold and hot sinks, and induces a temperature gradient $\partial T/\partial z$ in the region of the system. Compared with the no-equilibrium molecular dynamics (NEMD) approach,[38,39] which imposes a temperature gradient on the system to measure the resulting heat flux, RNEMD applies the heat flux, obtaining the temperature as the system's response. The thermal conductivity of the system, κ, is then determined by Fourier's law:

$$\kappa = -\frac{\sum_{i=1}^{N} \frac{m}{2}(v_{\mathrm{ih}}^2 - v_{\mathrm{ic}}^2)}{2tL_xL_y\langle \partial T/\partial z\rangle}, \tag{1}$$

where v_{ih} and v_{ic} refer to the velocity of the atoms involved in the kinetic energy exchange in the cold and hot sinks, respectively. The sum i is taken over all steps N during the swap of atoms in the heat sinks; m denotes the mass of particles involved in the exchange. The lengths L_x and L_y denote the cross-sectional area of the simulation box in the x and y directions, respectively. The temperature gradient $\langle \partial T/\partial z\rangle$ is linearly fitted from the temperature profile along the heat flow. The denominator 2 accounts for the two directions of heat flux from the middle heat source due to the periodical boundary conditions.

The conventional Tersoff bond-order potential[40] has been employed with respect to the bonds in the Si-NWs. A time step of 0.5 fs was selected so as to guarantee energy conservation over simulation times of several tens of nanoseconds, and to include higher frequency vibrations. Having relaxed the system for approximately 2 ns, using a Berendsen thermostat[41] at a given temperature, we continue to relax the system with a microcanonical ensemble for another 200 ps to ensure that the system has reached a state of equilibrium. Thereafter, a constant heat flux is applied using the Müller–Plathe RNEMD method[35,36] to establish a steady state of heat flow, depending on the number of atoms and the different structures. Finally, we maintain an additional 5 ns time evolution of the system under steady state conditions, in order to obtain the cumulative mean values of the heat flux. The temperature profile is averaged based on the kinetic energies for each slice, measured every 100 ps.

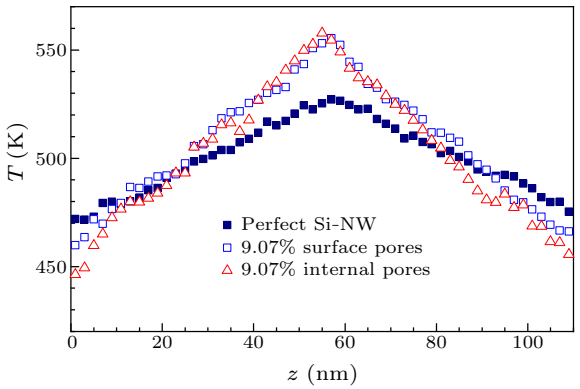

Fig. 2. Typical temperature profiles of different configurations of Si-NWs, as denoted in the figure during RNEMD simulations.

Figure 2 shows a typical example of temperature profiles along the nanowire with porosity of 9.07% for surface and internal pores, respectively. The temperature profile between the hot sink and the cold sinks can be linearly fitted separately. The temperature gradients $\langle \partial T/\partial z\rangle$ can be obtained from the fitted slope. The exchange rate of kinetic energy between heat source and heat sink, approximately every 500–2000 time steps, generates a steady temperature gradient with approximate values of 1.12, 1.59, and 1.84 K/nm, based on the perfect Si-NW and Si-NWs with 9.07% surface pores and 9.07% internal pores, respectively.

Results and Discussions. The temperature dependence of thermal conductivity in perfect and patterned Si-NWs, respectively, is shown in Fig. 3. Owing to the enhanced phonon-phonon Umklapp scattering,[25] the thermal conductivity of the perfect Si-NW exhibits a slow decay with increasing temperature of $1/T^{\alpha}$, which is consistent with existing experimental[42] and theoretical[25] observations. By contrast, the thermal conductivity of the patterned Si-NWs shows a very slow reduction rate, and tends to be almost constant over the full temperature range studied, which is in agreement with previous experimental results.[12,14] This is a typical behavior related to the temperature dependence[25,43] of thermal conductivity in disordered or alloy systems, resulting from elastic phonon scattering.[43] It is generally assumed[44] that the phonon scattering rate in elastic structure defects, $\tau_{\rm d}^{-1}$, can be described as $\tau_{\rm d}^{-1} \sim D \cdot \omega^4$, where D is the coefficient and ω is the angular frequency of the phonon mode. Although greater populations of high-frequency phonons are excited at higher temperatures, the phonon scattering rate $\tau_{\rm d}^{-1}$ increases rapidly with ω^4. Thus high-frequency phonons contribute little to thermal conductivity at high temperatures.

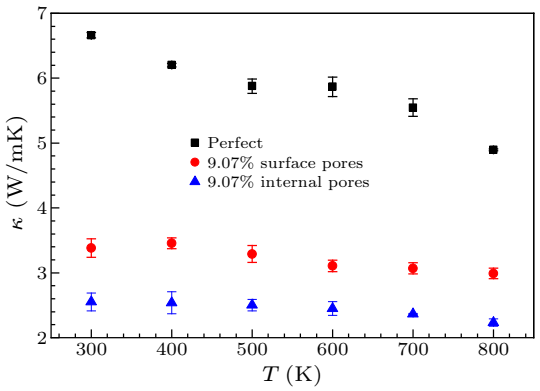

Fig. 3. Temperature dependence of the thermal conductivity of the perfect Si-NW and Si-NWs with surface pores and internal pores, respectively.

Another significant feature in Fig. 3 is that the thermal conductivity of the Si-NW with the internal pores is much lower than that with surface pores. The smaller value of thermal conductivity in the Si-NW with internal pores may imply that the scattering of phonons from internal body defects is stronger than that from surface structures. To explore the mechanism of this stronger phonon scattering behavior, we have calculated the vibrational density of state (VDOS) and the phonon-mode participation. The corresponding results of the VDOS and the phonon-mode participation are shown in Figs. 4(a) and 4(b), respectively. Here, the VDOS is calculated from the power spectrum of the auto-correlation of velocity. The phonon-mode participation for each phonon mode, p_λ, is defined[45] as

$$P_\lambda = \frac{\sum_{i,\alpha} \varepsilon_{i,\alpha}^{\lambda *} \varepsilon_{i,\alpha}^{\lambda}}{n \sum_{i,\alpha} (\varepsilon_{i,\alpha}^{\lambda *} \varepsilon_{i,\alpha}^{\lambda})^2}, \tag{2}$$

where n is the number of atoms in the supercell, and $\varepsilon_{i,\alpha}^{\lambda}$ is the displacement eigenvector for the ith atom of the λ phonon mode in the $\alpha, \alpha = x, y, z$ directions. The phonon mode participation estimates the fraction of atoms participating in a certain phonon mode, denoting whether a particular phonon mode is localized ($p \to 1/n$) or delocalized ($p \to 1$).

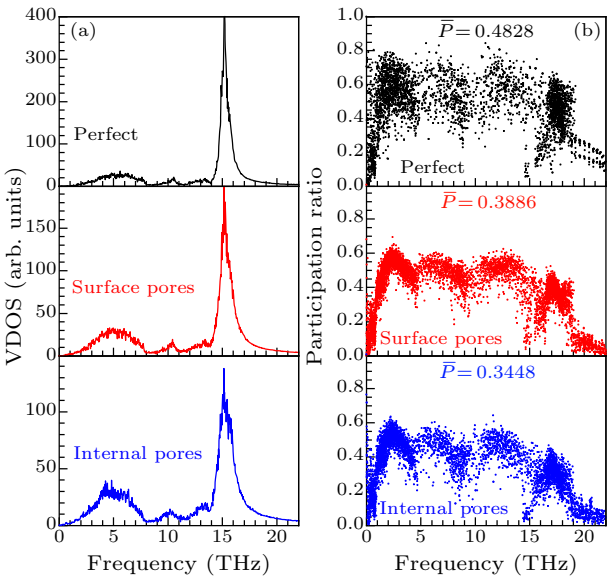

Fig. 4. (a) Vibrational density of states (VDOS) as a function of frequency. (b) Phonon mode-participation versus frequency. The structural configuration as indicated in the figures includes a perfect Si-NW (upper panel), an Si-NW with surface pores (the middle panel) and an Si-NW with internal pores (lower panel).

Figure 4(a) demonstrates the typical VDOS for the three models: the perfect Si-NW and the nanostructured Si-NWs with surface/internal pores. As shown in the figure, for a diamond-structured crystal of silicon, the longitudinal and two transverse optical phonons are triply degenerate at the value of phonon wave vector $q = 0$, yielding a single peak in the Raman spectrum, as indicated by the highest peak around 15.6 THz in Fig. 4(a). However, a lot of dangling bonds appear for the nanostructured Si-NWs. The major peak of the VDOS for the surface Si atoms can be found[25] at around 5 THz. In our simulation, we have also verified that these peaks of vibration state for dangling atoms at the surface are also located at around 5 THz. It can be observed from Fig. 4(a) that the relative ratio of the peak around 5 THz to the Raman peak around 15.6 THz for nanostructured wires is substantially enhanced, as compared with the perfect nanowire. In other words, many vibrational states of dangling atoms become apparent with the appearance of pores in the nanowire. Based on this figure, we also

find that the relative ratio of VDOS around 5 THz for the atoms in the internal pores is slightly larger than that for the pores at the wire's surface.

The corresponding phonon mode-participation ratio is also shown in Fig. 4(b) as a function of frequency. We find that the phonon modes in the low-frequency range have larger values of participation ratio, suggestive of a propagating property for these modes. By contrast, phonon modes at higher frequencies, for example above 17 THz, have smaller values of participation ratio, indicating a localization property for these modes. The averaged values of the participation ratio over all phonon modes, $\overline{P}$, for the perfect wire and the patterned wires with surface pores and internal pores, respectively, are also indicated in Fig. 4(b). The smaller value, $\overline{P} = 0.3448$, for the Si-NW with internal pores may indicate a more strongly localized property for these phonon modes, resulting from localized vibrations in the surface dangling atoms, as compared with a value of $\overline{P} = 0.3886$ for surface pores.

To sum up, the smaller value of thermal conductivity of Si-NWs with internal pores may be ascribed to both the stronger vibrational states from the dangling bonds of surface atoms, and the localized property of non-propagating phonon modes. Next, we investigate the relation to thermal conductivity of nanostructured Si-NWs, which is essential for tuning the thermal conductivity of nanowires[12,13] in experiments.

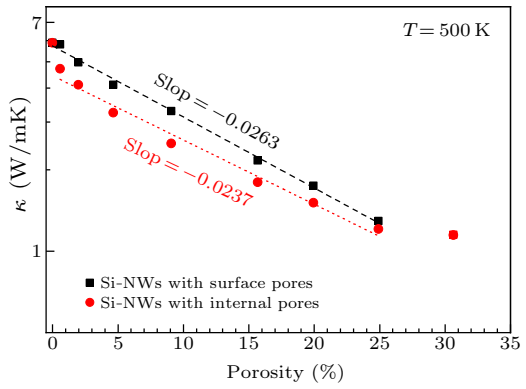

Fig. 5. Thermal conductivity of Si-NWs with surface pores and internal pores as a function of porosity.

In Fig. 5, we plot the thermal conductivity of Si-NWs with surface pores and internal pores, respectively, as a function of porosity. We find that the thermal conductivity of Si-NWs with the internal pores is greater than that of wires with surface pores, below a porosity level of about 25%. The reason for this lower value of thermal conductivity in Si-NWs with internal pores is the same as that discussed in the above paragraph. To quantify the dependence of thermal conductivity on the porosity of pores, a semi-log plot of thermal conductivity as a function of porosity is given in Fig. 5. Based on this, an exponential decay of thermal conductivity κ with porosity $n_{\rm p}$ can clearly be assumed, as $\kappa \propto \exp(-\beta n_{\rm p})$. This exponential decay of thermal conductivity with porosity is qualitatively validated by experimental observations,[12] where thermal conductivity decays exponentially with the irradiation dose. The discrepancy between these results and those of a previous report, which details a power-law decay[46] in thermal conductivity with porosity, may result from the definition of vacancy, and the details of the specific simulations employed. Our fitted parameter $n_{\rm p}$, denoting exponential decay, is shown in the figure. The decay rate $n_{\rm p} = 0.0263$ for Si-NWs with surface pores, while $n_{\rm p} = 0.0237$ for Si-NWs with internal pores, which demonstrates a slower decay rate of thermal conductivity in comparison with nanowires with surface pores.

Furthermore, in the region of high porosity, we discover a transition porosity at around 25%, above which the thermal conductivity of both types of patterned Si-NW tend to be very close, approaching the amorphous limit of $\sim$1 W/mK.[12] This behavior agrees with previous reports.[12,14,25,46] Here, the primary heat carrier may be diffusion,[47,48] primarily composed of non-propagating and delocalized modes.

In conclusion, using the molecular dynamics method, we have found that the thermal conductivity of Si-NWs with internal pores is greater than that in nanowires with surface pores, below a porosity of about 25%. This can be ascribed to both the stronger vibrational states from the dangling bonds of surface atoms, and the localized property of non-propagating phonon modes, which may bear some resemblance to the resonant structures in branched Si-NWs.[49,50] Based on our simulations, an exponential decay of thermal conductivity with porosity is proposed as $\kappa \propto \exp(-\beta n_{\rm p})$ in the low-porosity range. In the range of high porosity beyond 25%, we find that the thermal conductivity of Si-NWs approaches the amorphous limit, and is insensitive to specific phonon scattering processes. Our results should contribute to a better understanding of the process of tuning thermal conductivity in Si-NWs by means of patterned nanostructures, and may provide some valuable insights into the optimal design of thermoelectric materials.

References

[1] Hicks L D and Dresselhaus M S 1993 *Phys. Rev. B* **47** 12727
[2] Majumdar A 2004 *Science* **303** 777
[3] Rurali R 2010 *Rev. Mod. Phys.* **82** 427
[4] Chen R, Lee J, Lee W and Li D 2019 *Chem. Rev.* **119** 9260
[5] Zhou W X, Cheng Y, Chen K Q, Xie G F, Wang T and Zhang G 2020 *Adv. Funct. Mater.* **30** 1903829
[6] Zeng Y J, Wu D, Cao X H, Zhou W X, Tang L M and Chen K Q 2020 *Adv. Funct. Mater.* **30** 1903873
[7] Zeng Y J, Wu D, Cao X H, Feng Y X, Tang L M and Chen K Q 2020 *J. Mater. Chem. A* **8** 11884
[8] Chen X K and Chen K Q 2020 *J. Phys.: Condens. Matter* **32** 153002
[9] Hochbaum A I, Chen R K, Delgado R D, Liang W J, Gar-

nett E C, Najarian M, Majumdar A and Yang P D 2008 *Nature* **451** 163
[10] Boukai A I, Bunimovich Y, Tahir-Kheli J, Yu J K, Goddard W A and Heath J R 2008 *Nature* **451** 168
[11] Zhao Y S, Yang L N, Kong L Y, Nai M H, Liu D, Wu J, Liu Y, Chiam S Y, Chim W K, Lim C T, Li B W, Thong J T L and Hippalgaonkar K 2017 *Adv. Funct. Mater.* **27** 1702824
[12] Zhao Y S, Liu D, Chen J, Zhu L Y, Belianinov A, Ovchinnikova O S, Unocic R R, Burch M J, Kim S, Hao H F, Pickard D S, Li B W and Thong J T L 2017 *Nat. Commun.* **8** 15919
[13] Weisse J M, Marconnet A M, Kim D R, Rao P M, Panzer M A, Goodson K E and Zheng X L 2012 *Nanoscale Res. Lett.* **7** 554
[14] Lim J W, Hippalgaonkar K, Andrews S C, Majumdar A and Yang P D 2012 *Nano Lett.* **12** 2475
[15] Zianni X 2018 *J. Phys. D* **51** 114003
[16] Shahraki M G and Zeinali Z 2015 *J. Phys. Chem. Solids* **85** 233
[17] Kang B and Estreicher S K 2014 *Phys. Rev. B* **89** 155409
[18] Wang Z, Ni Z H, Zhao R J, Chen M H, Bi K D and Chen Y F 2011 *Physica B* **406** 2515
[19] da C C C A, Termentzidis K, Chantrenne P and Kleber X 2011 *J. Appl. Phys.* **110** 034309
[20] Liu L and Chen X 2010 *J. Appl. Phys.* **107** 033501
[21] Wang J and Wang J S 2007 *Appl. Phys. Lett.* **90** 241908
[22] Volz S G and Chen G 1999 *Appl. Phys. Lett.* **75** 2056
[23] Nakamura Y 2018 *Sci. Technol. Adv. Mater.* **19** 31
[24] Yang N, Zhang G and Li B 2008 *Nano Lett.* **8** 276
[25] Hu M and Poulikakos D 2012 *Nano Lett.* **12** 5487
[26] Wingert M C, Chen Z C Y, Dechaumphai E, Moon J, Kim J H, Xiang J and Chen R K 2011 *Nano Lett.* **11** 5507
[27] Donadio D and Galli G 2009 *Phys. Rev. Lett.* **102** 195901
[28] Dettori R, Melis C, Cartoixa X, Rurali R and Colombo L 2015 *Phys. Rev. B* **91** 054305
[29] Yang L, Yang N and Li B W 2014 *Nano Lett.* **14** 1734
[30] Chen J, Zhang G and Li B W 2010 *Nano Lett.* **10** 3978
[31] Yu J K, Mitrovic S, Tham D, Varghese J and Heath J R 2010 *Nat. Nanotechnol.* **5** 718
[32] Xiong S Y, Kosevich Y A, Saaskilahti K, Ni Y X and Volz S 2014 *Phys. Rev. B* **90** 195439
[33] Zhou Y G and Hu M 2016 *Nano Lett.* **16** 6178
[34] Zhang Z W, Ouyang Y L, Cheng Y, Chen J, Li N B and Zhang G 2020 *Phys. Rep.* **860** 1
[35] Müller-Plathe F 1997 *J. Chem. Phys.* **106** 6082
[36] Zhang M M, Lussetti E, de Souza L E S and Muller-Plathe F 2005 *J. Phys. Chem. B* **109** 15060
[37] Plimpton S 1995 *J. Comput. Phys.* **117** 1
[38] Zeng Y J, Liu Y Y, Zhou W X and Chen K Q 2018 *Chin. Phys. B* **27** 036304
[39] Chen X K, Liu J, Xie Z X, Zhang Y, Deng Y X and Chen K Q 2018 *Appl. Phys. Lett.* **113** 121906
[40] Tersoff J 1989 *Phys. Rev. B* **39** 5566(R)
[41] Berendsen H J C, Postma J P M, Gunsteren W F V, DiNola A and Haak J R 1984 *J. Chem. Phys.* **81** 3684
[42] Li D Y, Wu Y Y, Kim P, Shi L, Yang P D and Majumdar A 2003 *Appl. Phys. Lett.* **83** 2934
[43] Donadio D and Galli G 2010 *Nano Lett.* **10** 847
[44] Klemens P G 1955 *Proc. Phys. Soc. A* **68** 1113
[45] Joseph L F M D K, Allen P B and Wooten F 1993 *Phys. Rev. B* **48** 12589
[46] Lee Y, Lee S and Hwang G S 2011 *Phys. Rev. B* **83** 125202
[47] Wingert M C, Kwon S, Hu M, Poulikakos D, Xiang J and Chen R K 2015 *Nano Lett.* **15** 2605
[48] Larkin J M and McGaughey A J H 2014 *Phys. Rev. B* **89** 144303
[49] Hussein M I, Tsai C N and Honarvar H 2020 *Adv. Funct. Mater.* **30** 1906718
[50] Xiong S Y, Saaskilahti K, Kosevich Y A, Han H X, Donadio D and Volz S 2016 *Phys. Rev. Lett.* **117** 025503